Reformation of rippled quasi-parallel shocks: 2-D hybrid simulations

Yufei Hao[1,2,3], Xinliang Gao[1,3] (iD), Quanming Lu[1,3] (iD), Can Huang[1,3], Rongsheng Wang[1,3] (iD), and Shui Wang[1,3]

[1]CAS Key Laboratory of Geospace Environment, Department of Geophysics and Planetary Science, University of Science and Technology of China, Hefei, China, [2]State Key Laboratory of Space Weather, Chinese Academy of Sciences, Beijing, China, [3]Collaborative Innovation Center of Astronautical Science and Technology, Harbin, China

Abstract One-dimensional (1-D) hybrid simulations have demonstrated that a quasi-parallel shock is nonstationary and undergoes a reformation process. Recently, two-dimensional (2-D) hybrid simulations have revealed that ripples along the shock front is an inherent property of a quasi-parallel shock. In this paper, we investigate reformation process of a rippled quasi-parallel shock with a 2-D hybrid simulation model. The simulation results show that at a rippled shock, incident particles behave differently and just can be partially reflected at some specific locations along the rippled shock front, and the reflected particles will form an ion beam that moves back to the upstream along the magnetic field. Then, the beam locally interacts with upstream waves, and the waves are enhanced and finally steepen into a new shock front. As the upstream incident plasma moves to the shock front, the new shock front will approach and merge with the old shock front. Such a process occurs only before these locations along the shock front, and after the merging of the new shock front and old shock front is finished, a relatively plane shock front is formed. Subsequently, a new rippled shock front is again generated due to its interaction with the upstream waves, and it will repeat the previous process. In this pattern, the shock reforms itself quasiperiodically, and at the same time, ripples can shift along the shock front. The simulations present a more complete view of reformation for quasi-parallel shocks.

1. Introduction

Collisionless shocks are of much concern and considered to be important sources of power law spectra of energetic particles in space and astrophysical plasma [*Axford et al.*, 1977; *Blandford and Ostriker*, 1978; *Bell*, 1978; *Webb et al.*, 1995; *Gedalin et al.*, 2016]. Shocks can be separated into two groups by the shock angle θ_{Bn} (defined as the angle between the shock normal and the upstream background magnetic field): quasi-perpendicular shocks ($\theta_{Bn} > 45^{\circ}$) and quasi-parallel shocks ($\theta_{Bn} < 45^{\circ}$) [*Jones and Ellison*, 1991]. Particles show different behaviors at a quasi-perpendicular shock and at a quasi-parallel shock. At a quasi-perpendicular shock, which has a distinguishable magnetic structure including foot, ramp and overshoot, a part of upstream incident particles can be reflected and quickly transmit into the downstream [*Leroy et al.*, 1982; *Sckopke et al.*, 1983; *Hada et al.*, 2003; *Lembège et al.*, 2004; *Ofman et al.*, 2009; *Yang et al.*, 2009a, 2009b, 2012; *Guo and Giacalone*, 2010; *Ofman and Gedalin*, 2013; *Hao et al.*, 2014; *Gedalin*, 2016a, 2016b, 2016c; *Johlander et al.*, 2016b; *Tsubouchi et al.*, 2016]; also, some reflected particles may travel along the background magnetic field to further upstream and lead to an ion foreshock [*Meziane et al.*, 2004; *Mazelle et al.*, 2005; *Savoini et al.*, 2013]. At a quasi-parallel shock, backstreaming particles generated by reflection can move far upstream along the background magnetic field, and then they will interact with upstream incident particles, resulting in the excitation of ultralow frequency (ULF) waves with oblique propagation [*Burgess*, 1989; *Scholer and Burgess*, 1992; *Lucek et al.*, 2002, 2004, 2008; *Tsubouchi and Lembège*, 2004; *Eastwood et al.*, 2005a, 2005b; *Omidi et al.*, 2004, 2005; *Wilson et al.*, 2013; *Shan et al.*, 2014, 2016; *Wu et al.*, 2015; *Hao et al.*, 2016a, 2016b; *Johlander et al.*, 2016a]. These waves will be convected back to shock front due to their smaller phase velocity compared to the incident plasma velocity [*Burgess*, 1989; *Scholer et al.*, 1993, 2003; *Guo and Giacalone*, 2013; *Blanco-Cano et al.*, 2006, 2009; *Su et al.*, 2012a, 2012b; *Liu et al.*, 2016a, 2016b].

Using a 1-D hybrid simulation model, *Burgess* [1989] reported that a quasi-parallel shock shows a cyclic behavior and reform itself periodically. After that, the reformation of quasi-parallel shocks has been explained by several mechanisms, such as dissipation of whistler waves at shock front [*Lyu and Kan*, 1990], interface instability between upstream incident plasma, and thermalized downstream particles [*Winske et al.*, 1990]

and deflection of specularly reflected particles by upstream waves [*Onsager et al.*, 1991; *Scholer and Burgess*, 1992]. Further investigation with 1-D hybrid simulations shows that reflected particles indeed play a crucial role in the reformation process [*Scholer*, 1993]. Reflected particles can form a cold ion beam [*Su et al.*, 2012b] in the upstream at the beginning of the reformation, and this beam will be deflected by the upstream wave crest convected toward the shock front [*Su et al.*, 2012b]. Then, particles from the deflected beam are quickly trapped between the upstream waves and shock front and get accelerated [*Su et al.*, 2012a]. Part of them obtain sufficiently high energy to escape further upstream and become superthermal diffuse ions [*Su et al.*, 2012b]. In such a process, the upstream waves grow and steepen gradually due to the increase of number density of diffuse ions as they approach the shock front [*Scholer*, 1993; *Su et al.*, 2012b]. When arriving in the immediate upstream, by deflecting the cold ion beam, the waves may steepen into a new shock front [*Onsager et al.*, 1991; *Scholer and Burgess*, 1992; *Scholer et al.*, 1993; *Su et al.*, 2012b], which will exceed the old shock front in amplitude. Finally, the new shock front merges with the old shock front, and a reformation cycle is finished.

With 2-D hybrid simulations, reformation process had once been confirmed, and *Thomas et al.* [1990] suggest that cyclic behavior is an inherent property of quasi-parallel shocks rather than a result of restriction of spatial dimensions as in 1-D simulations. In the process of reformation, upstream waves generated due to the ion-ion beam instability will be brought into the quasi-parallel shock front and form ripples [*Schwartz and Burgess*, 1991; *Scholer et al.*, 1993], which has the local curvature variations along the shock front. Recently, at a rippled shock, *Hao et al.* [2016a, 2016b] investigated ion dynamics and evolution of the quasi-parallel shock with hybrid simulations, which are performed with a larger spatial and temporal scale compared to a work [*Scholer et al.*, 1993] where the reformation is described as a coherent process without consideration of effect of ripples along the shock front. Their results show different ion dynamics along the rippled shock front: (i) on some parts of ripples, incident particles can be directly transmitted more easily and form downstream high-speed jets, which had been observed by satellites in terrestrial magnetosheath [*Savin et al.*, 2008; *Hietala et al.*, 2009, 2012; *Archer et al.*, 2012; *Archer and Horbury*, 2013; *Hietala and Plaschke*, 2013; *Plaschke et al.*, 2013] and are thought to contribute to the formation of the downstream secondary shock [*Hietala et al.*, 2009] and throat aurora [*Han et al.*, 2016, 2017]; (ii) but, particles tend to be reflected and accelerated on other parts, where a large-amplitude electric field exists and points toward upstream [*Hao et al.*, 2016b]. According to the closed relationship between reflected particles and generation of new shock front as described in 1-D works [*Scholer*, 1993; *Su et al.*, 2012b], reformation process along a 2-D rippled quasi-parallel shock should not be coherent. *Hao et al.* [2016a] found that the reformation of a quasi-parallel shock is intermittent and takes place with a certain time range. Here, in this paper, we introduce a new scenario of reformation of a quasi-parallel shock in two-dimensional space.

We organized this paper as follows. In section 2, the hybrid simulation model is described and associated parameters are presented. The simulation results are shown in section 3. Conclusions and discussion are given in section 4.

2. Simulation Model

A two-dimensional hybrid simulation model is used to investigate the process of reformation at quasi-parallel shocks. Hybrid simulations treat electrons as massless fluid and regard ions as macroparticles. The plasma consists of electron and proton components which are denoted as e and p, respectively. Charge neutrality is assumed and the background magnetic field B_0 lies in the x-y simulation plane. Initially, the injected plasma moves to the right rigid boundary with a fixed bulk velocity $V_{inj} = 4.5V_A$ (where V_A is the upstream Alfven speed). It is reflected by the right boundary and will interact with continuously injected plasma, which results in the formation of a shock front. In the downstream reference frame, the propagating velocity of the shock is about $1.0V_A$ that points to the left along x direction. Therefore, the Alfven Mach number of the shock is about 5.5. Its shock angle is $\theta_{Bn} = 30°$, and the upstream plasma beta is $\beta_p = \beta_e = 0.4$. In this simulation, the number of grid cell is $n_x \times n_y = 1000 \times 300$ and the grid sizes are $\Delta x = 0.5c/\omega_{pi}$ and $\Delta y = 1.0c/\omega_{pi}$ (where c is the speed of light and ω_{pi} is the ion plasma frequency under upstream parameters). And periodic boundary condition is used in the y direction. The electron resistivity length is set to be $L_\eta = \eta c^2/(4\pi V_A) = 0.1$, where η indicates the interactions between particles and high-frequency waves. The time step is $\Omega_i \Delta t = 0.02$ (where $\Omega_i = eB_0/m$ is the ion frequency). These parameters are the same as those used in *Hao et al.* [2015, 2016a].
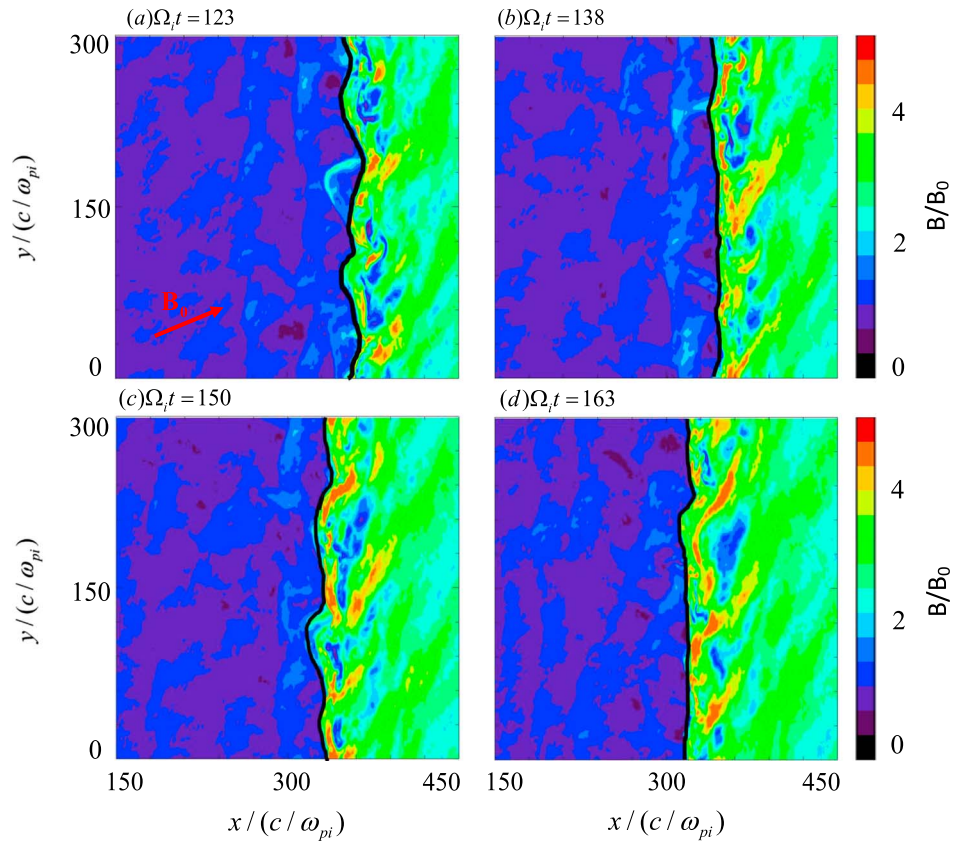
Figure 1. The total magnetic fields and sketches of shock front at times $\Omega_i t$= (a) 123, (b) 138, (c) 150, and (d) 163, in which black bold lines indicate the sketches of the shock fronts.

However, *Hao et al.* [2015, 2016a] emphasized the formation of high-speed jets in the downstream, and in this paper we will study the reformation process of a rippled quasi-parallel shock.

3. Simulation Results

Figure 1 illustrates an overview of total magnetic fields, and we also plot the profiles of the shock front with black bold lines. In Figure 1a, ripples exist along the shock front, and we can see several filamentary magnetic structures in the immediate downstream. Later, the rippled shock front transforms into a relatively plane shock front whose ripples have a smaller amplitude as shown in Figure 1b, and then the plane shock front changes back to a rippled shock front at $\Omega_i t = 150$. As in Figure 1d, the shock front can be plane again after a time period at $\Omega_i t = 163$. Therefore, it seems that in 2-D space, the quasi-parallel shock exhibits a new cyclic behavior, which is different from a cyclic reformation process in 1-D simulations performed by *Burgess* [1989]. With 1-D hybrid simulations, *Burgess* [1989] pointed out that quasi-parallel shocks can present a cyclic behavior, which shows periodical evolution of magnetic field. And such a reformation process takes place in 1-D space and just shows a periodical change of a simple 1-D magnetic structure of the shock. Here, by using a 2-D hybrid simulation code, the quasi-parallel shock shows some magnetic structures that cannot exist in 1-D simulations, such as upstream waves in 2-D space, ripples along the shock front, and filamentary magnetic structures in the immediate downstream, so that we can clearly reveal the evolution of quasi-parallel shocks.

In this paper, a ripple is defined as an arched structure along the shock front as shown in Figure 2 (left), and its scale is about $75c/\omega_{pi}$ in the direction of y. We divide the ripple into two parts: the upper and lower parts, as described in Figure 2. At the same time, to further investigate the amplitude of the shock front and magnetic structures, three cuts along x axis are selected at three different y values $y = 186c/\omega_{pi}$, $149c/\omega_{pi}$, and $121c/\omega_{pi}$, indicated by black dashed lines. The corresponding magnetic field profiles are presented in Figure 2 (right),
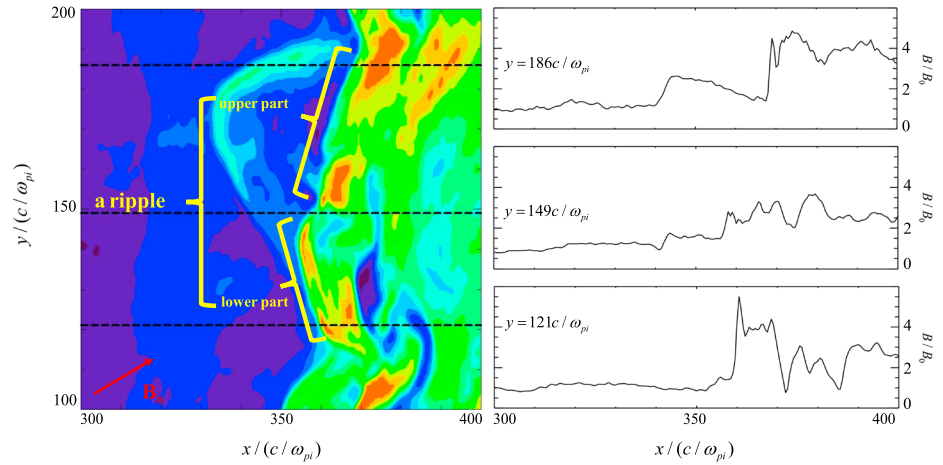
Figure 2. (left) Contour plot of magnetic field zoomed at a large-scale ripple at time $\Omega_i t = 123$ and three cuts along x axis at $y = 186c/\omega_{pi}$, $149c/\omega_{pi}$ and $121c/\omega_{pi}$. (right) Profiles of magnetic field along the three cuts.

respectively. From Figure 2 (right), we can find that their profiles and amplitude of the shock front are not exactly the same: at $y = 186c/\omega_{pi}$ and $121c/\omega_{pi}$, the shock front is a sharp jump, while at $y = 49c/\omega_{pi}$ there is a slope in the shock front and its spatial scale in x direction is large, and the amplitude of peak in the shock front ranges from $5B_0$ to $2.7B_0$ from the top to the bottom panels.

In previous studies with 1-D hybrid simulations [*Scholer*, 1993; *Su et al.*, 2012a], the major role of the reflected particles in quasi-parallel shocks had been confirmed in the formation of the new shock front. Therefore, given the close relationship between the new shock front and reflected particles at quasi-parallel shocks, we follow a group of particles restricted in the upstream area to study the ion dynamics in the shock. Their positions in the simulation plane are plotted in Figure 3 with total magnetic field at times $\Omega_i t = 100$, $\Omega_i t = 121.5$, and $\Omega_i t = 188.5$, respectively. We select all the injected particles located in an area ($250c/\omega_{pi} < x < 270c/\omega_{pi}$, $0c/\omega_{pi} < y < 300c/\omega_{pi}$) at $\Omega_i t = 100$, which is illustrated in Figure 3a. They will confront the shock front at time $\Omega_i t = 121.5$ and begin to interact with it. During their interaction for a time period from $\Omega_i t = 121.5$ to $\Omega_i t = 188.5$, some particles can be reflected by the shock front and the others are directly transmitted into downstream, and finally a part of particles move back to upstream and become backstreaming particles that are located before the red dashed line, which is at $x = 290c/\omega_{pi}$ and roughly denotes the shock front. Then, to clearly understand the evolution of these backstreaming particles, they are selected and traced as they interact with the shock front, and results are presented in Figure 4, where their positions are displayed at the same times as in Figure 3. At the time $\Omega_i t = 100$, these backstreaming particles are located together in the upstream in Figure 4a and then separate into several groups when they move close to the shock front. At time $\Omega_i t = 121.5$, each group of them reaches the shock front, and almost all groups encounter a lower part of a ripple. At last, these particles naturally go back upstream and form ion
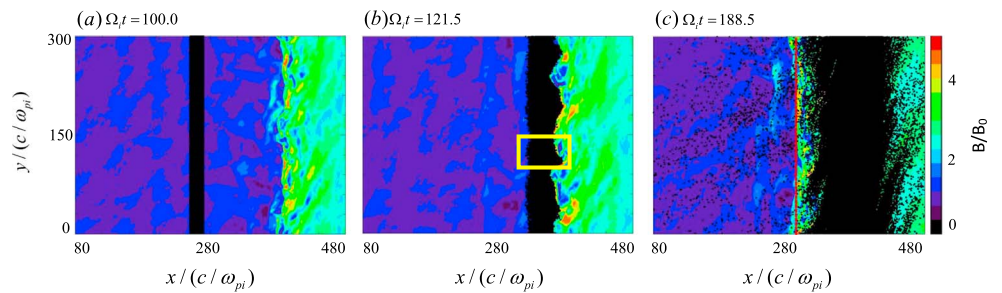

Figure 3. The time evolution of particles at times $\Omega_i t = 100.0$, 121.5, and 188.5. The particles are restricted in the area ($250c/\omega_{pi} < x < 270c/\omega_{pi}$, $0c/\omega_{pi} < y < 300c/\omega_{pi}$) at time (a) $\Omega_i t = 100$, and backstreaming particles are that located in upstream at time (c) $\Omega_i t = 188.5$, where the red dashed line is set to be the position of the shock front. (b) The yellow box denotes the area ($310c/\omega_{pi} < x < 370c/\omega_{pi}$, $114c/\omega_{pi} < y < 141c/\omega_{pi}$).
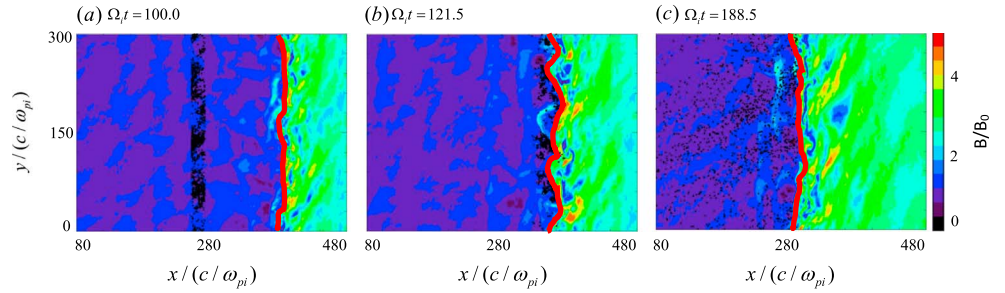
Figure 4. The time evolution of backstreaming particles from Figure 2c at times $\Omega_i t=$ (a) 100, (b) 121.5, and (c) 188.5 with total magnetic fields for reference. The red bold lines indicate the shock front in Figures 4a–4c.

beams moving to the further upstream along background magnetic field as shown in Figure 4c. That is consistent to the results of the previous investigation where incident particles are easier to be reflected back to upstream at lower part of a ripple due to a large amplitude electric field in the shock normal direction [*Hao et al.*, 2016b]. In other words, the scenario is that incident particles can be easily reflected at the lower portion of each ripple along the shock front, and the reflected particles may interact with upstream waves locally in immediate upstream, which means new shock fronts may be formed locally in front of the shock.

Then, in order to investigate the local interaction of reflected particles with upstream waves, a part of particles is selected in the area indicated in Figure 3b by a yellow box ($310c/\omega_{pi} < x < 370c/\omega_{pi}, 114c/\omega_{pi} < y < 141c/\omega_{pi}$) around the lower part of a ripple at the shock front. Detailed analysis of these particles is displayed in Figure 5, where their average velocity is plotted in top panels with white arrows in the simulation plane, as well as the evolution of sketches of the shock front in the bottom panels at times $\Omega_i t=$ (a) 121.5, (b) 130.0, (c) 142.0, and (d) 150.0. At the beginning of the evolution of the selected particles, in Figure 5 top panels, they are located around the lower part of the ripple and begin to interact with the shock at time $\Omega_i t = 121.5$, we can see a wave crest at about $x = 335c/\omega_{pi}$. After a time period as shown at $\Omega_i t = 130$, these particles are separated into two parts including reflected and transmitted particles, and at the same time the wave crest locally forms a new shock front indicated by a yellow line labeled N1 in the immediate upstream accompanied with deflection of the reflected beam along the new shock front. Then, a part of these reflected
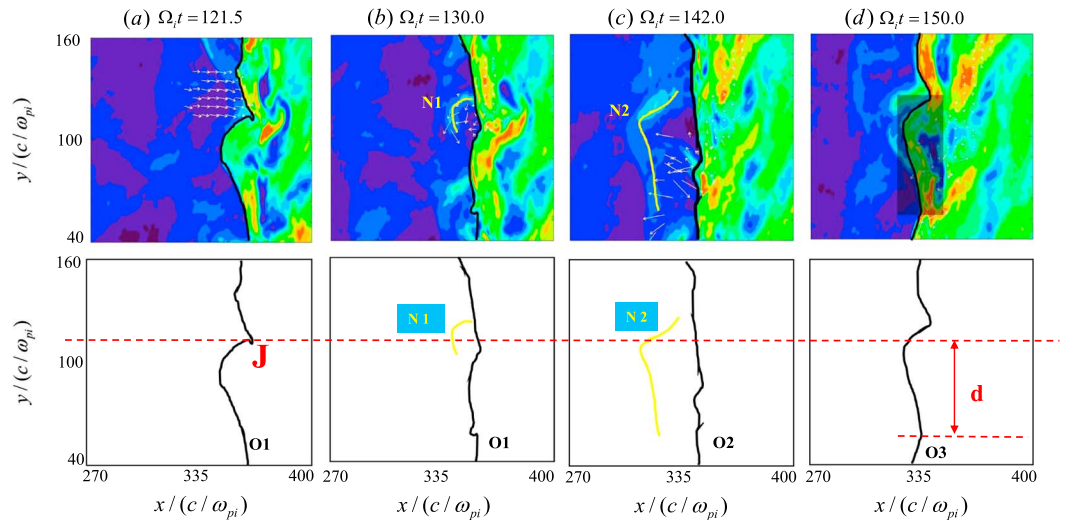

Figure 5. The time evolution of average velocity of selected particles and the shock front at times $\Omega_i t=$ (a) 121.5, (b) 130.0, (c) 142.0, and (d) 150.0. These particles are located in the yellow box in Figure 2b, and their average velocity is shown with white arrows in the top panels. The evolution of sketches of shock fronts is indicated in the bottom panels, where N1 and N2 with yellow solid lines denote new shock fronts and O1–O3 with black solid lines represent the shock front. The red dashed lines in the bottom panels are used to indicate the location of joints denoted by J between ripples, and d is defined as the distance ripples shifting for.
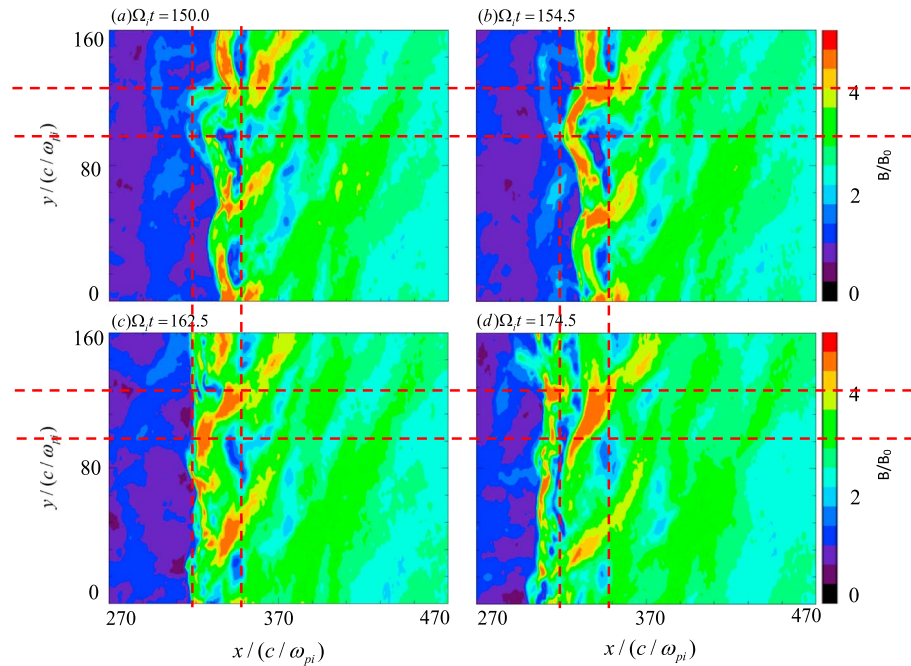
Figure 6. Zoomed in view of the total magnetic fields in simulation plane at four times $\Omega_i t$= (a) 150.0, (b) 154.5, (c) 162.5, and (d) 174.5. Red dashed lines are used to indicate the location of the upper part of a ripple as a reference.

particles escape to the further upstream when the new shock N1 merges with the shock front and interacts again with the upstream waves. The interaction, to some extent, makes contribution to the formation of another new shock front N2 at time $\Omega_i t = 142.0$. At last, the N2 also merges with the shock front and become a visible ripple at the time $\Omega_i t = 152.0$. The process takes a time period $\sim 28\Omega_i^{-1}$, which can be treated as a self-reformation time of the 2-D quasi-parallel shock. From Figure 5 bottom panels, where new shock fronts are indicated by N1 and N2 and old shock front denoted with O1, O2, and O3, we find that the new shock front N1 merges with the rippled shock front O1 at a joint denoted by J between two ripples, and then the rippled shock front O1 becomes a relatively plane shock front O2. On the contrary, that the new shock front N2 merges with the plane shock front O2 leads to the formation of a rippled shock front O3, and the new shock front N2 forms a large-scale ripple along the shock front O3. Finally, according to the positions of two joints between ripples denoted with two red dashed lines at times $\Omega_i t = 121.5$ and $\Omega_i t = 150$, we can know that the ripples shifted to the $-y$ direction along the shock front for a distance of d, which is roughly equal to the scale of a ripple $\sim 75c/\omega_{pi}$. And, considering the process takes about $28\Omega_i^{-1}$, the shifting speed of the ripples along the shock front can be estimated as about $2.6V_A$. As to the new shock front N2, the contribution of the particles, which are escaped from N1 and shown with white arrows before the shock front in Figure 5c, is not enough to its formation; instead, other reflected particles generated at the shock front O2 might be necessary to facilitate the formation of the new shock front N2, and these particles should be mainly located in the area without white arrows between N2 and the shock front in the Figure 5 top panels when the time is around $\Omega_i t = 142$.

Particles can be easily reflected at the lower portion of a ripple but tend to directly transmit the shock front at the upper portion of a ripple [Hao et al., 2016b]. Therefore, the evolution of the upper part of a ripple along the shock front should be different from that of the lower part. We also studied the evolution of the upper portion of the ripple, and the result is illustrated in Figure 6, where the total magnetic fields are plotted in the simulation domain at four times $\Omega_i t$= (a) 150.0, (b) 154.5, (c) 162.5, and (d) 174.5. Each panel in this figure plots the total magnetic field zoomed around the large-scale ripple at the shock, and the red dashed lines are used to focus on the upper part of the ripple. At the beginning of the generation of the ripple in Figure 6a, its amplitude is not so large until the ripple becomes mature at time $\Omega_i t = 154.5$. Then, in Figure 6c, the shock front becomes a nearly plane shock front, and at the same time the upper part of the original ripple evolves into downstream and becomes a downstream filamentary magnetic structure. As shown in Figure 6d, this
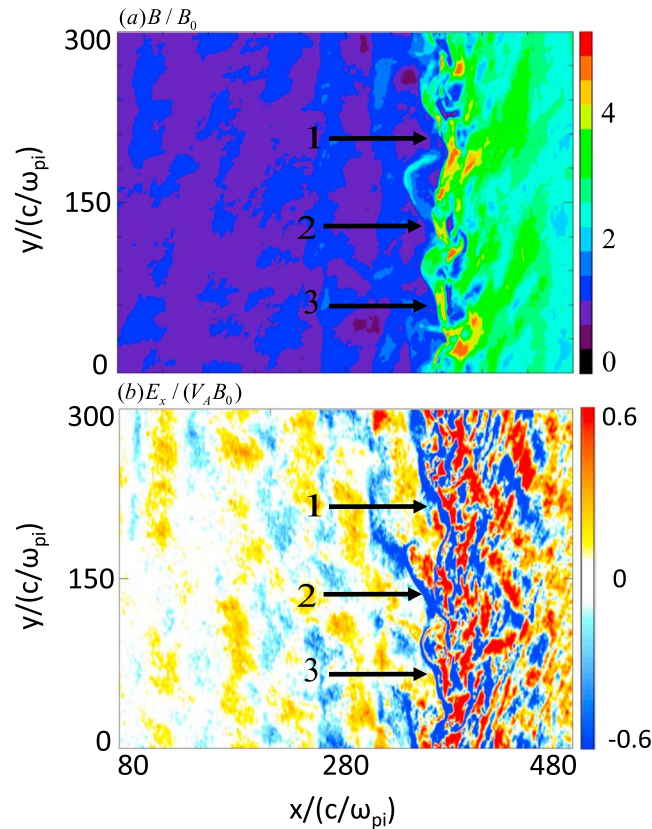
Figure 7. (a) The total magnetic field and (b) the x component of electric field in the simulation plane at time $\Omega_i t = 121.5$. "1," "2," and "3" with arrows denote the lower parts of three ripples.

portion of the original ripple persists for an extended time period till farther downstream with a large amplitude after the ripple became mature. As presented by previous paper [*Hao et al.*, 2016b], at the upper part of a ripple, particles can directly transmit into the downstream and form a high-speed jet. In other words, reflection and particle acceleration, which are directly relevant to the supercritical shock dissipation process, almost cannot occur at the upper part of the ripples, and finally, the parts of the ripples can last till downstream and become downstream filamentary magnetic structures.

As described above, ion dynamics and evolution of shock front on the two sides of the ripples are different, and that is attributed to the different electric fields along the shock front [*Su and Lu*, 2012; *Hao et al.*, 2016b]. Especially, *Su and Lu* [2012] pointed out that electric field in the normal direction at the shock front plays a critical role in partially reflecting incident particles back to upstream. Therefore, in Figure 7, we plot the x component electric field at time $\Omega_i t = 121.5$ when the ripples along the shock front are visible and also plot the total magnetic field as a reference in the simulation plane. We can see that at the lower parts of ripples indicated by black arrows with numbers 1–3, where particles are easier to be reflected, large-amplitude x component electric structures exist and point to upstream, and it can be clearly seen that upstream waves make great contributions to the formation of the large-scale electric fields along the shock front. And, to further analyze electric fields, we also plot a zoomed view of E_x around a large-scale ripple and electric field profiles of three cuts along x axis at different y values in Figure 8. In Figure 8 (left), these cuts are selected at three fixed location $y = 186 c/\omega_{pi}$, $156 c/\omega_{pi}$, and $121 c/\omega_{pi}$, which are denoted by black dashed lines. The profiles of electric fields along the three cuts are illustrated in Figure 8 (right), respectively. As shown in these panels, there always have a negative spiky E_x denoted by $a - c$ with arrows in the shock front, while in Figure 8 (right middle) another negative spiky E_x indicated by d exists at $x \sim 338 c/\omega_{pi}$ in the upstream and is thought to be the electric field brought by upstream waves. Further, in Figure 8 (right bottom), a large-scale electric structure labeled e convected back by the upstream waves connects the negative spiky E_x in the shock front, which facilitates the reflection of incident particles. The combination of the electric field brought back by the upstream waves and the electric field in the shock front will influence the ion dynamic when the upstream waves interact with the quasi-parallel shock front [*Hao et al.*, 2016b]. Thus, it is reasonable that ion dynamics along the shock front behave differently, and that incident particles can be easily reflected just at some specific locations, which also means that reflected beams can also be formed at a plane shock front.

Moreover, to try to eliminate the restriction of the scale of the simulation plane in y direction and confirm the existence of the ripples along quasi-parallel shocks, a new run is performed with the same parameters as the above simulation but with a larger y scale $L_y = n_y \times \Delta y = 450 \times 1.0 c/\omega_{pi} = 450 c/\omega_{pi}$. The results are displayed in Figure 9, which plots the total magnetic field in the simulation domain at two times $\Omega_i t = 153.0$ and 170.0. In Figure 9a, we can see that ripples exist along the shock front and have an estimated scale in y direction, which is around $75 c/\omega_{pi}$ and in good agreement with the scale in Figure 1. Then, at $\Omega_i t = 170$, the rippled
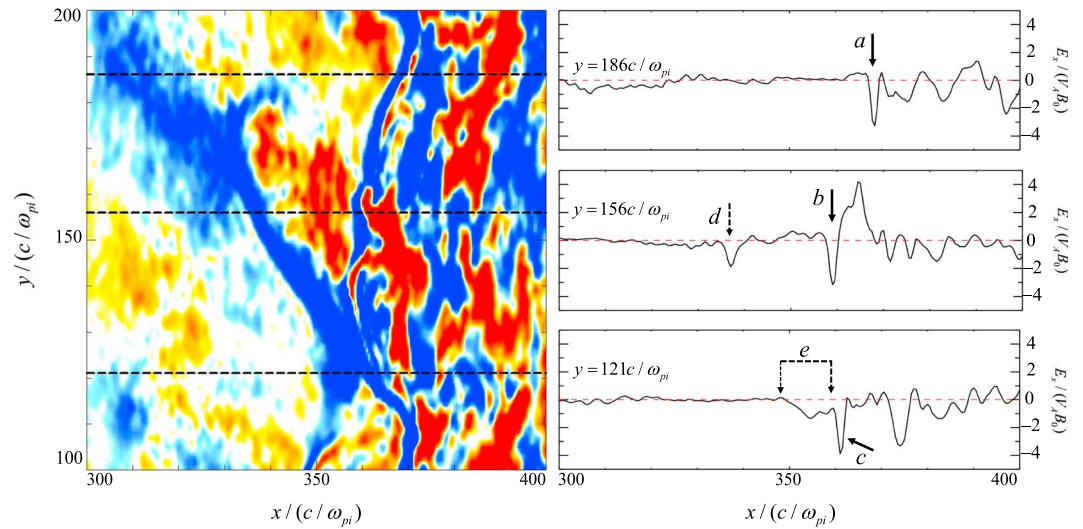
Figure 8. (left) Contour plot of electric field zoomed at a large-scale ripple at time $\Omega_i t = 121.5$ and three cuts along the x axis at $y = 186c/\omega_{pi}$, $156c/\omega_{pi}$, and $121c/\omega_{pi}$. (right) Profiles of electric field along the three cuts. $a - c$ indicate the negative spiky E_x in the shock front and $d - e$ denote the electric structures brought back by the upstream waves.

shock evolves into a relatively plane shock front that has relatively small amplitude ripples. Therefore, ripples should be inherent structures at quasi-parallel shocks, and a rippled shock front can indeed transform into a plane shock.

To confirm that reflected particles can move back upstream along the background magnetic field as shown in Figure 5, we changed the direction of the upstream background magnetic field from $\mathbf{B} = \left(B_x \hat{i}, B_y \hat{j}, 0 \right)$ to $\mathbf{B} = \left(B_x \hat{i}, -B_y \hat{j}, 0 \right)$ in the simulation model. The result of this new run is illustrated in Figure 10, which shows the evolution of a group of particles selected as that in Figure 5. It can be seen that after interaction of these particles with the shock, a part of them is reflected and moves back to upstream along the background magnetic field, which is reverse in y direction compared to the original case. Therefore, reflected particles can indeed move back upstream along the background magnetic field.

As a summary, we present a sketch of the reformation process in Figure 11. In Figure 11a, new shock fronts N1 are locally generated before a rippled shock. Then, the new shock fronts merge with the rippled shock,
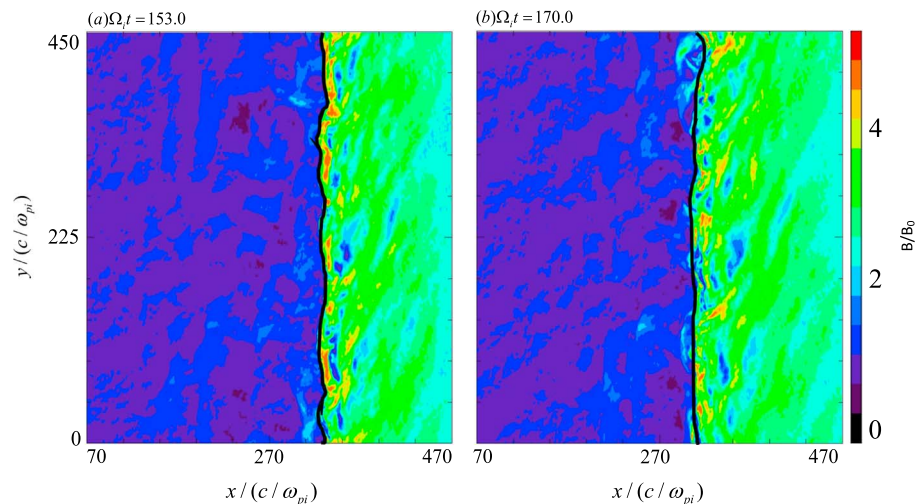

Figure 9. The total magnetic field in simulation plane at 2 times (a) $\Omega_i t = 153.0$ and (b) $\Omega_i t = 170.0$ from a new run with an increased y scale $L_y = n_y \times \Delta y = 450 \times 1.0c/\omega_{pi} = 450c/\omega_{pi}$ based on parameters in simulation model. Black bold lines denote the profile of the shock front in each panel.
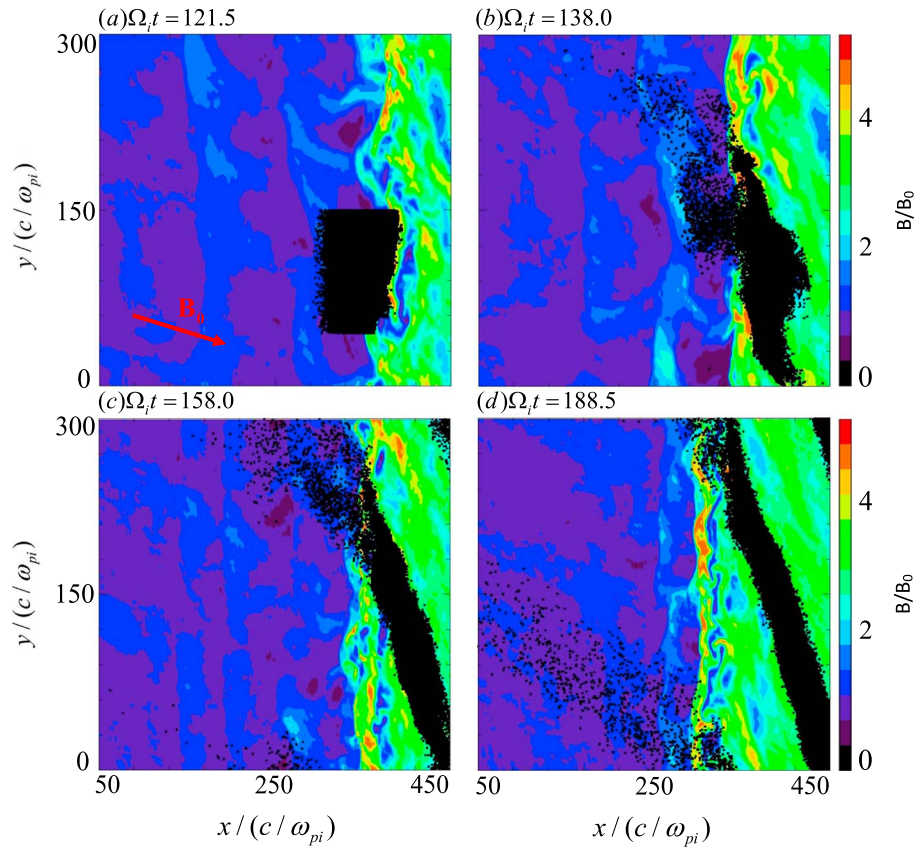
Figure 10. Positions of a group of particles located at the upper part of a ripple at times $\Omega_i t=$ (a) 121.5, (b) 138.0, (c) 158.0, and (d) 188.5 from a new run, which has a reversed magnetic field in y direction compared to the case in the simulation model. The red arrow indicates the upstream background magnetic field.

resulting in a plane shock front in Figure 11b. Meanwhile, before the plane shock, new shock fronts N2 are also locally formed due to the interaction of upstream waves with the reflected ion beams from the plane shock. Finally, the new shock fronts N2 merge with the plane shock front, resulting in a rippled shock in turn as shown in Figure 11c. And we can see that the ripples shift along the shock front for a distance.

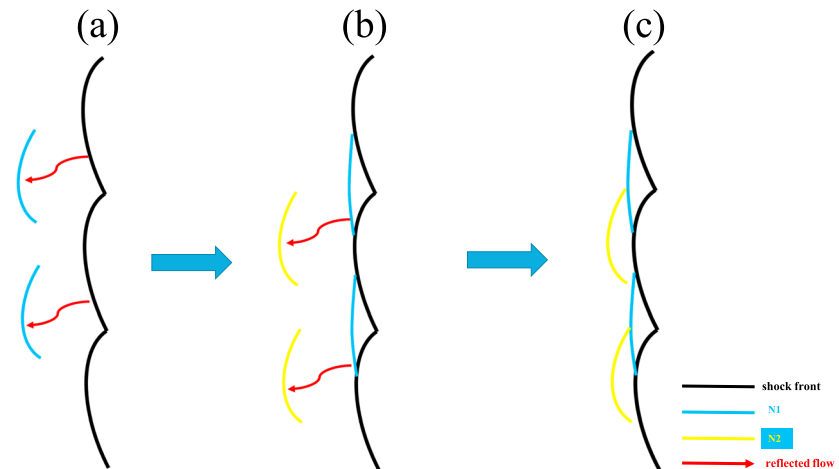
Figure 11. The sketch for evolution of shock front. (a) A rippled shock front, (b) a plane shock front, and (c) a rippled shock front. Solid lines and red arrows denote shock front and reflected beams, and N1 and N2 indicate new shock fronts.

4. Conclusions and Discussion

In this paper, with a 2-D hybrid simulation mode, we have studied the reformation process of ripped quasi-parallel shocks. Our simulations show that reflected beams can be generated at the lower part of ripples due to the existence of large-scale electric fields pointing to the upstream, and they will move to the upstream along the background magnetic field. Then, these beams interact with the approaching upstream waves and facilitate the formation of local new shock fronts that will merge with the old shock at each joints between ripples. Such a process results in a plane shock front. Afterward, at the plane shock, reflected beams may also be formed, and the beams can locally interact with upstream waves, producing local new shock fronts. Ultimately, the new shock fronts merge with the plane shock, and a new rippled shock is generated in turn. During the quasiperiodic reformation of the shock, the ripples are found to shift along the shock front to a considerable distance.

Also, one thing that should be noted is that the cross-shock electrostatic potential along a quasi-parallel shock front consists of electric fields generated in shock front and that convected into the shock by the upstream waves. The waves are excited by the interaction of backstreaming particles and incident particles and convected by incident flow toward the shock. Their propagation direction is found oblique to the upstream background magnetic field [*Eastwood et al.*, 2005a, 2005b; *Blanco-Cano et al.*, 2006, 2009]. Therefore, the upstream waves will bring electric fields into the shock, resulting in different electric structures and ion dynamics along the shock front no matter it is rippled or relatively plane. Further, it is reasonable that the cyclic reformation processes resulted from local reflection of incident particles are not coherent along the quasi-parallel shocks, and the spatial scale of ripples depends on the wavelength of upstream waves.

Scholer et al. [1993] suggested that reformation process is synchronous along shock front in 2-D hybrid simulations, where the spatial scale is limited under previous computational power, so that the effect of ripples has not been taken into account. Here we performed 2-D hybrid simulations with larger spatial and temporal scale to investigate the evolution of a rippled quasi-parallel shock and find that reformation processes are spatial and temporal cyclic behavior, as well as temporal evolution as shown at 1-D shock. With 2-D hybrid simulations, *Hao et al.* [2016a] found that the upstream waves can interact with the shock front and form downstream filamentary magnetic structures when they get downstream immediately. As described in our results, incident particles tend to be reflected at the lower part of the ripples, which means energy dissipation of shock front mainly occurs at these positions. Therefore, we can imagine that parts of the shock front around the upper part of the ripples, where incident particles can be directly transmitted into downstream, will last till downstream and form filamentary magnetic structures.

References

Archer, M. O., and T. S. Horbury (2013), Magnetosheath dynamic pressure enhancements: Occurrence and typical properties, *Ann. Geophys.*, *31*, 319–331, doi:10.5194/angeo-31-319-2013.

Archer, M. O., T. S. Horbury, and J. P. Eastwood (2012), Magnetosheath pressure pulses: Generation downstream of the bow shock from solar wind discontinuities, *J. Geophys. Res.*, *117*, A05228, doi:10.1029/2011JA017468.

Axford, W. I., E. Leer, and G. Skadron (1977), The acceleration of cosmic rays by shock waves, paper presented at 15th International Cosmic Ray Conference, Bulg. Acad. of Sci., Plovdiv, Bulgaria, 13–26 Aug.

Bell, A. R. (1978), The acceleration of cosmic rays in shock fronts. I, *Mon. Not. R. Astron. Soc.*, *182*, 147–156.

Blanco-Cano, X., N. Omidi, and C. T. Russell (2006), Macrostructure of collisionless bow shocks: 2. ULF waves in the foreshock and magnetosheath, *J. Geophys. Res.*, *111*, A10205, doi:10.1029/2005JA011421.

Blanco-Cano, X., N. Omidi, and C. T. Russell (2009), Global hybrid simulations: Foreshock waves and cavitons under radial IMF geometry, *J. Geophys. Res.*, *114*, A01216, doi:10.1029/2008JA013406.

Blandford, R. D., and J. P. Ostriker (1978), Particle acceleration by astrophysical shocks, *Astrophys. J.*, *221*(1), L29–L32, doi:10.1086/182658.

Burgess, D. (1989), Cyclic behavior at quasi-parallel collisionless shocks, *Geophys. Res. Lett.*, *16*(5), 345–348, doi:10.1029/GL016i005p00345.

Eastwood, J. P., A. Balogh, E. A. Lucek, C. Mazelle, and I. Dandouras (2005a), Quasi-monochromatic ULF foreshock waves as observed by the four-spacecraft Cluster mission: 1. Statistical properties, *J. Geophys. Res.*, *110*, A11219, doi:10.1029/2004JA010617.

Eastwood, J. P., A. Balogh, E. A. Lucek, C. Mazelle, and I. Dandouras (2005b), Quasi-monochromatic ULF foreshock waves as observed by the four-spacecraft Cluster mission: 2. Oblique propagation, *J. Geophys. Res.*, *110*, A11220, doi:10.1029/2004JA010618.

Gedalin, M. (2016a), Downstream plasma parameters in laminar shocks from ion kinetics, *Phys. Plasmas*, *23*, 102904.

Gedalin, M. (2016b), Transmitted, reflected, quasi-reflected, and multiply reflected ions in low-Mach number shocks, *J. Geophys. Res. Space Physics*, *121*, 10,754–10,767, doi:10.1002/2016JA023395.

Gedalin, M. (2016c), Effect of alpha particles on the shock structure, *J. Geophys. Res. Space Physics*, *122*, 71–76, doi:10.1002/2016JA023460.

Gedalin, M., W. Dröge, and Y. Y. Kartavykh (2016), Dependence of the spectrum of shock-accelerated ions on the dynamics at the shock crossing, *Phys. Rev. Lett.*, *117*, doi:10.1103/PhysRevLett.117.275101.

Guo, F., and J. Giacalone (2010), Effect of large-scale magnetic turbulence on the acceleration of electrons by perpendicular collisionless shocks, *Astrophys. J.*, *715*, 406.

Guo, F., and J. Giacalone (2013), The acceleration of thermal protons at parallel collisionless shocks: Three-dimensional hybrid simulations, *Astrophys. J.*, *773*, 158.

Hada, T., M. Oonishi, B. Lembège, and P. Savoini (2003), Shock front nonstationarity of supercritical perpendicular shocks, *J. Geophys. Res.*, *108*(A16), 1233, doi:10.1029/2002JA009339.

Han, D.-S., H. Hietala, X.-C. Chen, Y. Nishimura, L. R. Lyons, J.-J. Liu, H.-Q. Hu, and H.-G. Yang (2017), Observational properties of dayside throat aurora and implications on the possible generation mechanisms, *J. Geophys. Res. Space Physics*, *122*, 1853–1870, doi:10.1002/2016JA023394.

Han, D.-S., Y. Nishimura, L. R. Lyons, H.-Q. Hu, and H.-G. Yang (2016), Throat aurora: The ionospheric signature of magnetosheath particles penetrating into the magnetosphere, *Geophys. Res. Lett.*, *43*, 1819–1827, doi:10.1002/2016GL068181.

Hao, Y., B. Lembege, Q. Lu, and F. Guo (2016a), Formation of downstream high-speed jets by a rippled nonstationary quasi-parallel shock: 2-D hybrid simulations, *J. Geophys. Res. Space Physics*, *121*, 2080–2094, doi:10.1002/2015JA021419.

Hao Y., Q. Lu, B. Lembege, C. Huang, M. Wu, F. Gou, L. Shan, J. Zheng, S. Wang (2015), Evidence of downstream high speed jets by a non-stationary and rippled front of quasi-parallel shock: 2-D hybrid simulations, paper presented at EGU General Assembly, Vienna, 12-17 Apr.

Hao, Y., Q. Lu, X. Gao, C. Huang, S. Lu, L. Shan, and S. Wang (2014), He^{2+} dynamics and ion cyclotron waves in the downstream of quasi-perpendicular shock: 2-D hybrid simulations, *J. Geophys. Res. Space Physics*, *119*, 3225–3236, doi:10.1002/2013JA019717.

Hao, Y., Q. Lu, X. Gao, and S. Wang (2016b), Ion dynamics at a rippled quasi-parallel shock: 2D hybrid simulations, *Astrophys. J.*, *823*, 7.

Hietala, H., and F. Plaschke (2013), On the generation of magnetosheath high-speed jets by bow shock ripples, *J. Geophys. Res. Space Physics*, *118*, 7237–7245, doi:10.1002/2013JA019172.

Hietala, H., T. V. Laitinen, K. Andreeova, R. Vainio, A. Vaivads, M. Palmroth, T. I. Pulkkinen, H. E. J. Koskinen, E. A. Lucek, and H. Reme (2009), Supermagnetosonic jets behind a collisionless quasiparallel shock, *Phys. Rev. Lett.*, *103*, 245,001, doi:10.1103/PhysRevLett.103.245001.

Hietala, H., N. Partamies, T. V. Laitinen, L. B. N. Clausen, G. Facsko, A. Vaivads, H. E. J. Koskinen, I. Dandouras, H. Reme, and E. A. Lucek (2012), Supermagnetosonic subsolar magnetosheath jets and their effects: From the solar wind to the ionospheric convection, *Ann. Geophys.*, *30*, 33–48, doi:10.5194/angeo-30-33-2012.

Johlander, A., A. Vaivads, Y. V. Khotyaintsev, A. Retino, and I. Dandouras (2016a), Ion injection at quasi-parallel shocks seen by the CLUSTER spacecraft, *Astrophys. J.*, *817*, L4.

Johlander, A., et al. (2016b), Rippled quasiperpendicular shock observed by magnetospheric multiscale spacecraft, *Phys. Rev. Lett.*, *117*, doi:10.1103/PhysRevLett.117.165101.

Jones, F. C., and D. C. Ellison (1991), The plasma physics of shock acceleration, *Space Sci. Rev.*, *58*(1), 259–346.

Lembège, B., J. Giacalone, M. Scholer, T. Hada, M. Hoshino, V. Krasnoselskikh, H. Kucharek, P. Savoini, and T. Terasawa (2004), Selected problems in collisionless-shock physics, *Space Sci. Rev.*, *110*, 161.

Leroy, M. M., D. Winske, C. C. Goodrich, C. S. Wu, and K. Papadopolous (1982), The structure of perpendicular bow shocks, *J. Geophys. Res.*, *87*(A7), 5081–5094, doi:10.1029/JA087iA07p05081.

Liu, T. Z., D. L. Turner, V. Angelopoulos, and N. Omidi (2016a), Multipoint observations of the structure and evolution of foreshock bubbles and their relation to hot flow anomalies, *J. Geophys. Res. Space Physics*, *121*, 5489–5509, doi:10.1002/2016JA022461.

Liu, T. Z., H. Hietala, V. Angelopoulos, and D. L. Turner (2016b), Observations of a new foreshock region upstream of a foreshock bubble's shock, *Geophys. Res. Lett.*, *43*, 4708–4715, doi:10.1002/2016GL068984.

Lucek, E. A., T. S. Horbury, M. W. Dunlop, P. J. Cargill, S. J. Schwartz, A. Balogh, P. Brown, C. Carr, K.-H. Fornaçon, and E. Georgescu (2002), Cluster magnetic field observations at a quasi-parallel bow shock, *Ann. Geophys.*, *20*, 1699–1710.

Lucek, E. A., T. S. Horbury, A. Balogh, I. Dandouras, and H. Rème (2004), Cluster observations of structures at quasi-parallel bow shocks, *Ann. Geophys.*, *22*, 2309–2314.

Lucek, E. A., T. S. Horbury, I. Dandouras, and H. Rème (2008), Cluster observations of the Earth's quasi-parallel bow shock, *J. Geophys. Res.*, *113*, A07S02, doi:10.1029/2007JA012756.

Lyu, L. H., and J. R. Kan (1990), Ion leakage, ion reflection, ion heating and shock-front reformation in a simulated supercritical quasi-parallel collisionless shock, *Geophys. Res. Lett.*, *17*(8), 1041–1044, doi:10.1029/GL017i008p01041.

Mazelle, C., K. Meziane, M. Wilber, and D. Le Queau (2005), Field-aligned and gyrating ion beams in a Planetary foreshock, in *The Physics of Collisionless Shocks: 4th Annual IGPP International Astrophysics Conference*, pp. 89–94, Am. Inst. of Phys., College Park, Md.

Meziane, K., et al. (2004), Simultaneous observations of field-aligned beams and gyrating ions in the terrestrial foreshock, *J. Geophys. Res.*, *109*, A05107, doi:10.1029/2003JA010374.

Ofman, L., and M. Gedalin (2013), Two-dimensional hybrid simulations of quasi-perpendicular collisionless shock dynamics: Gyrating downstream ion distributions, *J. Geophys. Res. Space Physics*, *118*, 1828–1836, doi:10.1029/2012JA018188.

Ofman, L. M., C. Balikhin, T. Russell, and M. Gedalin (2009), Collisionless relaxation of ion distributions downstream of laminar quasi-perpendicular shocks, *J. Geophys. Res.*, *114*, A09106, doi:10.1029/2009JA014365.

Omidi, N., X. Blanco-Cano, and C. T. Russell (2005), Macro-structure of collisionless bow shocks: 1. Scale lengths, *J. Geophys. Res.*, *110*, A12212, doi:10.1029/2005JA011169.

Omidi, N., X. Blanco-Cano, C. T. Russell, and H. Karimabadi (2004), Dipolar magnetospheres and their characterization as a function of magnetic moment, *Adv. Space Res.*, *33*(11), 1996–2003, doi:10.1016/j.asr.2003.08.041.

Onsager, T. G., D. Winske, and M. F. Thomsen (1991), Interaction of a finite-length ion beam with a background plasma—Reflected ions at the quasi-parallel bow shock, *J. Geophys. Res.*, *96*, 1775–1788, doi:10.1029/90JA02008.

Plaschke, F., H. Hietala, and V. Angelopoulos (2013), Anti-sunward high speed jets in the subsolar magnetosheath, *Ann. Geophys.*, *31*, 1877–1889, doi:10.5194/angeo-31-1877-2013.

Savin, S., et al. (2008), High kinetic energy jets in the Earth's magnetosheath: Implications for plasma dynamics and anomalous transport, *JETP Lett.*, *87*, 593–599, doi:10.1134/S0021364008110015.

Savoini, P., B. Lembege, and J. Stienlet (2013), On the origin of the quasi-perpendicular ion foreshock: Full-particle simulations, *J. Geophys. Res. Space Physics*, *118*, 1132–1145, doi:10.1002/jgra.50158.

Scholer, M. (1993), Upstream waves, shocklets, short large-amplitude magnetic structures and the cyclic behavior of oblique quasi-parallel collisionless shocks, *J. Geophys. Res.*, *98*, 47–57, doi:10.1029/92JA01875.

Scholer, M., and D. Burgess (1992), The role of upstream waves in supercritical quasi-parallel shock re-formation, *J. Geophys. Res.*, *97*(A6), 8319–8326, doi:10.1029/92JA00312.

Scholer, M., M. Fujimoto, and H. Kucharek (1993), 2-dimensional simulations of supercritical quasi-parallel shocks—Upstream waves, downstream waves and shock re-formation, *J. Geophys. Res.*, *98*, 18,971–18,984, doi:10.1029/93JA01647.

Scholer, M., H. Kucharek, and I. Shinohara (2003), Short large-amplitude magnetic structures and whistler wave precursors in a full-particle quasi-parallel shock simulation, *J. Geophys. Res.*, *108*(A7), 1273, doi:10.1029/2002JA009820.

Schwartz, S. J., and D. Burgess (1991), Quasi-parallel shocks: A patchwork of three-dimensional structures, *Geophys. Res. Lett.*, *18*, 373–376, doi:10.1029/91GL00138.

Sckopke, N., G. Paschmann, S. J. Bame, J. T. Gosling, and C. T. Russell (1983), Evolution of ion distributions across the nearly perpendicular bow shock: Specularly and non-specularly reflected-gyrating ions, *J. Geophys. Res.*, *88*(A8), 6121–6136, doi:10.1029/JA088iA08p06121.

Shan, L., C. Mazelle, K. Meziane, M. Delva, Q. Lu, Y. S. Ge, A. Du, and T. Zhang (2016), Characteristics of quasi-monochromatic ULF waves in the Venusian foreshock, *J. Geophys. Res. Space Physics*, *121*, 7385–7397, doi:10.1002/2016JA022876.

Shan, L., Q. Lu, M. Wu, X. Gao, C. Huang, T. Zhang, and S. Wang (2014), Transmission of large-amplitude ULF waves through a quasi-parallel shock at Venus, *J. Geophys. Res. Space Physics*, *119*, 237–245, doi:10.1002/2013JA019396.

Su, Y., and Q. Lu (2012), Cross-shock electrostatic potential and ion reflection in quasi-parallel supercritical collisionless shocks, *Chin. Phys. Lett.*, *29*(8), 089601.

Su, Y., Q. Lu, C. Huang, M. Wu, X. Gao, and S. Wang (2012a), Particle acceleration and generation of diffuse superthermal ions at a quasi-parallel collisionless shock: Hybrid simulations, *J. Geophys. Res.*, *117*, A08107, doi:10.1029/2012JA017736.

Su, Y., Q. Lu, X. Gao, C. Huang, and S. Wang (2012b), Ion dynamics at supercritical quasi-parallel shocks: Hybrid simulations, *Phys. Plasmas*, *19*, 092108.

Thomas, V. A., D. Winske, and N. Omidi (1990), Reforming super-critical quasi-parallel shocks, 1. One- and two-dimensional simulations, *J. Geophys. Res.*, *95*, 18,809–18,819, doi:10.1029/JA095iA11p18809.

Tsubouchi, K., and B. Lembège (2004), Full particle simulations of short large-amplitude magnetic structures (SLAMS) in quasi-parallel shocks, *J. Geophys. Res.*, *109*, A02114, doi:10.1029/2003JA010014.

Tsubouchi, K., T. Nagai, and I. Shinohara (2016), Stable ring beam of solar wind He^{2+} in the magnetosheath, *J. Geophys. Res. Space Physics*, *121*, 1233–1248, doi:10.1002/2015JA021769.

Webb, G. M., G. P. Zank, M. Ko, and D. J. Donohue (1995), Multidimensional Green's functions and the statistics of diffusive shock acceleration, *Astrophys. J.*, *453*, 178–206.

Wilson, L. B., III, A. Koval, D. G. Sibeck, A. Szabo, C. A. Cattell, J. C. Kasper, B. A. Maruca, M. Pulupa, C. S. Salem, and M. Wilber (2013), Shocklets, SLAMS, and field-aligned ion beams in the terrestrial foreshock, *J. Geophys. Res. Space Physics*, *118*, 957–966, doi:10.1029/2012JA018186.

Winske, D., N. Omidi, K. B. Quest, and V. A. Thomas (1990), Re-forming supercritical quasi-parallel shocks: 2. Mechanism for wave generation and front re-formation, *J. Geophys. Res.*, *95*(A11), 18,821–18,832, doi:10.1029/JA095iA11p18821.

Wu, M., Y. Hao, Q. Lu, C. Huang, F. Guo, and S. Wang (2015), The role of large amplitude upstream low-frequency waves in the generation of superthermal ions at a quasi-parallel collisionless shock: Cluster observations, *Astrophys. J.*, *808*, 2.

Yang, Z. W., Q. M. Lu, B. Lembège, and S. Wang (2009a), Shock front nonstationarity and ion acceleration in supercritical perpendicular shocks, *J. Geophys. Res.*, *114*, A03111, doi:10.1029/2008JA013785.

Yang, Z. W., Q. M. Lu, and S. Wang (2009b), The evolution of the electric field at a nonstationary perpendicular shock, *Phys. Plasmas*, *16*, 1.

Yang, Z. W., B. Lembège, and Q. M. Lu (2012), Impact of the rippling of a perpendicular shock front on ion dynamics, *J. Geophys. Res.*, *117*, A07222, doi:10.1029/2011JA017211.